MammoWave Breast Imaging Device: A Procedure for Device's Characterization Via Phantom Measurements and Subsequent Clinical Trials' Preliminary Results

Lorenzo Sani[1], Alessandro Vispa[1], Navid Ghavami[1], Daniel Álvarez Sánchez-Bayuela[1], Mario Badia[1], Alessandra Bigotti[1], Giovanni Raspa[1], Cristina Romero Castellano[2], Mohammad Ghavami[3], Gianluigi Tiberi[1,3]

[1]UBT - Umbria Bioengineering Technologies, Perugia, Italy,
[2]Virgin Health Hospital (Hospital Virgen de la Salud), Toledo, Spain,
[3]School of Engineering, London South Bank University, London, UK.

***Abstract*—The use of microwave imaging for breast cancer detection has witnessed growing attention from researchers around the globe. In the past decade, a number of microwave imaging prototypes have completed the preliminary experimental stages and reached clinical trials. This paper presents the machine characterization and preliminary clinical trial results of MammoWave, a dedicated radar-based microwave imaging system for breast lesion detection. MammoWave uses a Huygens principle-based algorithm, operates in air, using two antennas without requiring matching liquids. Our clinical trial results on 102 breasts from 64 patients indicate MammoWave's ability to distinguish between breasts with and without radiological findings, with a sensitivity of 88%. Significantly, when considering dense breasts only, the sensitivity does not decrease.**

Keywords—Microwave imaging, Huygens principle, Breast cancer detection

I. Introduction

The use of microwave imaging techniques for biomedical applications has attracted growing attention in recent decades. This is motivated due to the radiation-free nature of microwave imaging, in addition to its comfort and lower cost compared to current gold standards. One of the most common applications for such techniques is breast cancer detection, where the existing contrast in dielectric properties between normal and malignant tissues enables the possibility of detection and localization of lesions [1].

In the past decade, a number of microwave imaging prototypes have completed the preliminary experimental stages and reached clinical trials [2]. These prototypes are categorized into those using microwave tomography and those using radar-based techniques [3]. Tomographic algorithms attempt to reconstruct the dielectric property profiles of the tissues through inverse scattering, which may suffer from mathematical instability. Instead, radar methods solve a simpler problem of linearly reconstructing an image that represents a scattering map in arbitrary units.

Among one of the few radar-based prototypes that have reached clinical trials, MammoWave from UBT Srl has recently been undergoing trials in multiple European hospitals. MammoWave employs a Huygens principle-based algorithm [4], operates in air, using only two antennas without requiring matching liquids. Our previous works [5,6] have demonstrated the preliminary testing and clinical validation of the prototype both in phantoms and in clinical trials in hospitals in Italy. In this paper, we will describe the machine characterization procedure of MammoWave and subsequently present clinical trial results on 102 breasts from 64 patients. For each breast, the algorithm outputs conductivity weighted images in the form of intensity maps showcasing dielectric property homogeneity of the breast tissues. A number of image features are subsequently calculated and selected in order to quantify the non-homogenous behaviour of the breasts, allowing us to distinguish between breasts with no radiological findings (NF) and those with radiological findings (WF). Our output is then empirically compared with the corresponding radiologist review output gathered from mammography and/or MRI and/or echography.

The rest of the paper is outlined as follows. A brief description of the device and the HP algorithm is provided in Section II. MammoWave characterization procedure is described in Section III. Section IV presents the clinical trial results, while Section V concludes the paper.

II. Apparatus and Algorithm

The MammoWave device (Fig. 1) uses only one transmitting and one receiving antenna operating between 1 and 9 GHz (with 5 MHz sampling). The antennas, connected to a vector network analyzer (VNA) are installed at the same height, in free space and rotate around the azimuth collecting the microwave signals from different angular positions. The antennas are contained by a cylindrical hub, which is covered internally by absorbers. The hub includes a cup placed inside a hole, which permits the insertion of the patient's breast in a prone position (Fig. 1). S21 signals are recorded in a multi-bistatic fashion, such that for each transmitting position the receiving antenna is moved to measure at 80 receiving (rx) points (every 4.5°). We have 15 transmitting positions (tx),

This project has received funding from the European Union's Horizon 2020 research and innovation programme under grant agreement No 830265. This project leading to this application has received funding from the European Union's Horizon 2020 research and innovation programme under the Marie Sklodowska-Curie grant agreement No. 793449. This project has received funding from the European Union's Horizon 2020 research and innovation programme under the Marie Sklodowska-Curie grant agreement No. 872752.

displaced in 5 triplet sections centered at 0°, 72°, 144°, 216°, and 288°.

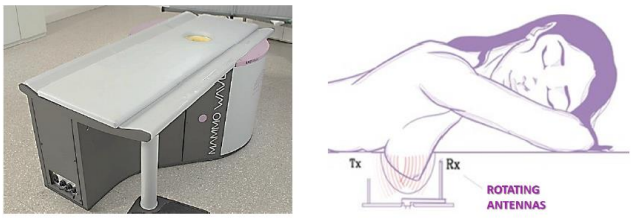

Fig. 1. Mammowave prototype (left), sketch of its breast scanning configuration (right).

Considering the movement of rx to measure the received signals at positions $\mathrm{rx}_{np} \equiv (a_0, \phi_{np}) \equiv \vec{\rho}_{np}$ along a circular surface with radius equal to a_0, the signal received may be represented as $S21_n^{m,p}(a_0, \phi_n; \mathrm{tx}_{m,p}; f)$, with m=1,2,…,5 being the transmitting sections, n=1,2,…,80 indicating the receiving positions and p=1,2,3, p'=1,2,3 representing the triplet number inside each transmitting section. Moreover, f is the frequency. The Huygens principle based algorithm is subsequently used to process the received signals and reconstruct the field inside the cylinder. In order to eliminate the possible artefacts, we perform a subtraction between S21 signals received from two measurements belonging to the triplet of the same transmitting section [5-6].

$$E_{\mathrm{HP,2D}}^{\mathrm{rcstr}} = \Delta_s \sum_{np=1}^{N_{PT}} (S21_n^{m,p} - S21_n^{m,p'}) G(k_1 |\vec{\rho}_{np} - \vec{\rho}\,|) \quad (1)$$

where k_1 indiscates the wave number (free-space), Δ_s denotes the spatial sampling and G represents 2D Green's function. In addition, the strings "rcstr" and "HP" stand for the reconstructed field, and the Huygens principle algorithm, respectively. Considering the use of N_F frequencies f_i, the final intensity image is achieved by incoherent addition of all the solutions from all frequency points and all transmitting sections.

$$I(\rho, \phi) = \sum_{m=1}^{5} \sum_{\substack{p=1 \\ p'=1 \\ p=p'}}^{3} \sum_{i=1}^{N_F} |E_{\mathrm{HP,2D}}^{\mathrm{rcstr}}|^2 \quad (2)$$

III. MammoWave Characterization

A thorough calibration and characterization procedure for any hardware machine is of utmost importance in order to maximize its accuracy and effectiveness. In this section, we will present examples of results from MammoWave's characterization procedure, examining its symmetry and repeatability.

To proceed with MammoWave characterization, we first performed a set of measurements with an empty machine (i.e., no phantom); next we prepared a homogenous phantom and performed a next set of measurements. Finally, phantoms with inclusions were prepared, where the inclusion was placed in different positions, with measurements being repeated for each location of the inclusion.

S11 and S22 parameters were measured for each scenario and their patterns within the investigated frequency range were plotted and analyzed. Additionally, several parameters were calculated to assess the effect of individual frequency bands on both the homogenous phantoms, and phantoms with inclusions.

As one of our repeatability tests, Fig. 2 shows the measurement of standard deviation (STD) for 15 different transmitting positions when considering all 80 receiving positions and 1600 frequency points. The measurement was replicated four times while keeping the number of receivers and frequency points unchanged. It can be observed that that the STD values are ~10^{-4}.

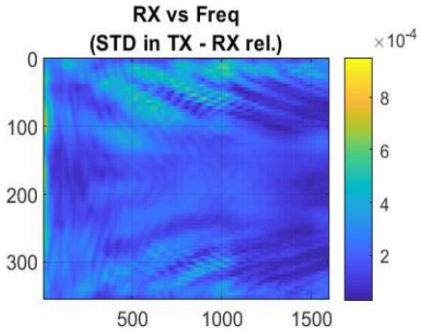

Fig. 2. Standard deviation plot of receiving positions (angle in deg) vs. frequency (number of sample). The measurement was replicated 4 times for each transmitting position.

Fig. 3 shows the maximum to average plot of a cylindrical oil phantom [5] with and without the inclusion. The inclusion, a 1 cm diameter cylindrical tube filled with water, was placed eccentrically at 4 different positions inside the oil phantom, each time moving its position by 90 degrees. For each position of the inclusion the measurement was repeated 3 times, considering all transmitting and receiving positions and all frequency points. Additionally, a homogeneous oil phantom measurement was also performed and repeated 4 times.

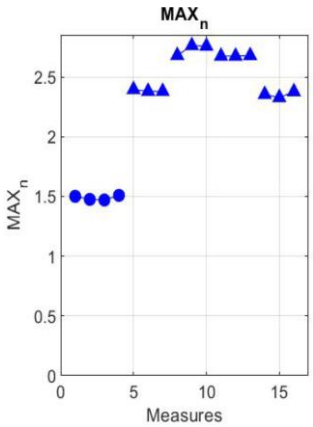

Fig. 3. Maximum to average plot examining the repeatability of an oil phantom with an inclusion placed at 4 different positions. Blue circles and triangles correspond to phantom oil phantom with and without water inclusion, respectively.

IV. Clinical Trial Results

To further evaluate the MammoWave system, a multicentric international clinical trial was approved in which microwave imaging was performed to patients that already went through conventional exams (ClinicalTrials.gov Identifier: NCT04253366). In this context, some preliminary results obtained in Hospital Virgen de la Salud, Toledo, Spain, are presented here. The resulting radiologists review

from these exams was used as gold standard for our investigation. Specifically, the radiologists review conventional exams for each patient that agrees to participate in the study, classifying the breasts into two groups: breasts with no radiological findings (NF) and breasts with radiological finding (WF); i.e., with lesions which could be either benign or malignant.

This investigation presents the outcomes of a first set of 102 breasts (27 NF and 75 WF), from 64 patients. The breasts examined had varying densities and radiological findings. The trials were performed in Toledo hospital, Spain, on female volunteers above 18 years old. For each breast, the radiologist study output was also obtained through either MRI, echography or mammography within the same month. All procedures and protocols followed those defined by institutional/national ethical standards and declaration of Helsinki (1964) and its subsequent amendments. All 64 volunteers read and signed the informative sheet and informed consent form before their trial.

The breast types were classified according the American college of radiology (ACR) scale. The scale ranges from ACR1 (extremely fatty) to ACR4 (extremely heterogeneous fibroglandular) [7]. Following this definition, breasts in the ACR3 and ACR4 category are classified as dense breasts here. The lesion types in our study included carcinoma, microcalcifications, fibroadenoma, cyst, nodule, among others [8-10].

Each participating volunteer was assisted by the clinical study coordinator, helping her with appropriately positioning the breast inside the cup (Fig. 1). Various cup sizes (all 1 mm thick) made of polylactic acid are available and are chosen according to the breast size for each exam [11]. Acquisition time for each breast takes around 10 minutes, during which no breast compression is applied. Subsequently, the microwave exam is completed, and a number of microwave images' features are calculated. Such features, used also in combination, are then used to allow distinction between NF and WF breasts, evaluating sensitivity and specificity versus gold standard.

No matching liquid was used at any time and hence the free space permittivity of 1 was used for image reconstruction. Meanwhile, the variation in the conductivity value from 0 to 0.9 S/m (0.1 sampling) was investigated for each breast, providing us with a set of conductivity-weighted images in the form of intensity maps in arbitrary units. Welsh's t-test with alpha=0.05 was performed, having a statistical significance set to $p<0.05$. For each feature of each conductivity-weighted image, the true positive (TP) and false negative (FN) rates were evaluated, enabling us to numerically calculate and plot the corresponding receiver operating characteristic (ROC) curves. From the ROC curves, the subsequent area under the curve (AUC) was thus determined. An example of ROC and AUC for maximum to average intensity ratio feature is shown in Fig. 6.

As test case examples, two breast images corresponding to a conductivity value of 0.3 S/m are shown here in more details. Microwave images, presented here in colour and normalized to unitary intensity average, are depicted here as 2D images in coronal (azimuthal) plane. They are divided into four quadrants corresponding to breast's Upper-Outer (UO), Upper-Inner (UI), Lower-Outer (LO) and Lower-Inner (LI) quadrants. In addition, one dimensional intensity projections on x and y are displayed in the inserts. X and y axes are in meters while intensity is in arbitrary units. For each of the two test cases, the output and main findings of the radiologist study review, together with the correspondent conventional images (mammography in this case), is also presented. Fig. 5 corresponds to a NF ACR3 breast from a 47 years old patient, while Fig. 6 shows a WF ACR2 breast from a 65 years old with invasive Ductal Carcinoma.

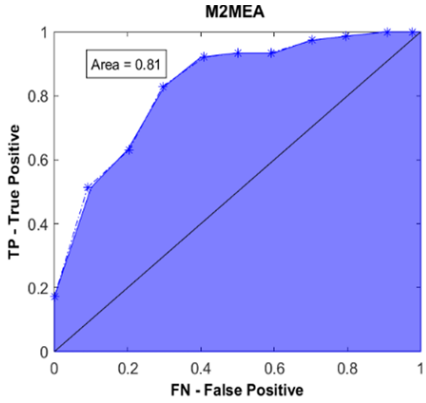

Fig. 4. Example of ROC and AUC for maximum to average intensity ratio (M2MEA) feature obtained from the microwave image.

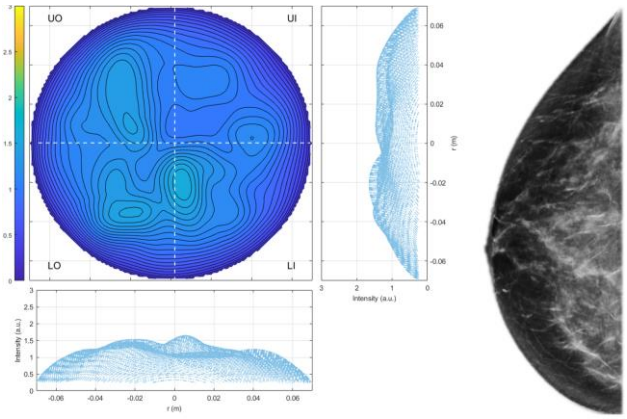

Fig. 5. Microwave image of a 47 years old healthy (NF) patient (ACR C), normalized to unitary average of the intensity for conductivity 0.3 S/m (left), corresponding mammography image of the same breast (right).

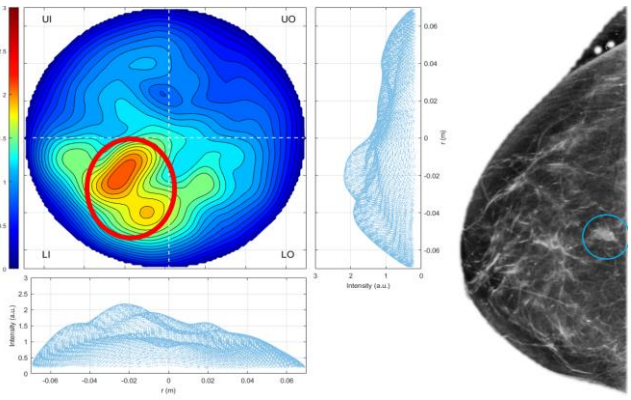

Fig. 6. Microwave image of a 65 years old pathologic (WF) patient (ACR B), normalized to unitary average of the intensity for conductivity 0.3 S/m (left), corresponding mammography BI-RADS 4C image of the same breast with confirmed invasive Ductal Carcinoma (right).

An appropriate combination of features (introduced empirically before the start of this prospective study) leads to sensitivity of 88%, specificity of 59.3% and accuracy of 80.4%. Sensitivity is maintained (85.3%) when considering dense breasts only, while specificity increases to an overall value of 90.0% and accuracy to 86.4%. Additional sensitivity results for benign and malignant findings, separately, are provided in Table I.

TABLE I. SENSITIVITY VALUES FOR THE BREASTS UNDER STUDY

	Sensitivity	**Sensitivity (dense breasts only)**
All WF breasts	66/75 (88.0%)	29/34 (85.3%)
Benign finding[a]	45/53 (86.8%)	25/29 (86.2%)
Malignant finding[b]	20/22 (90.9%)	4/5 (80.0%)

[a.] Duct ectasia, cysts, fibroadenoma, benign microcalcifications, architectural distortion (radial scar).

[b.] Confirmed carcinoma from nodules and/or architectural distortions.

V. CONCLUSIONS

This paper presented both the machine characterization procedure and clinical trial results of a novel microwave imaging prototype for breast cancer detection. Our results show that the presented microwave system has good overall sensitivity for breast lesion detection, and its performance does not decrease in patients with dense breast. Microwave imaging is a cheaper and safe technology that holds great promise in the future of breast cancer screening, as it is comfortable, sensitive, and is not affected by breast density. Its impact and implication can be especially noticeable in population-based screening programs to reduce over-diagnosis, interval cancer and healthcare costs by effective early-stage detection.

REFERENCES

[1] N. K. Nikolova, "Microwave imaging for breast cancer", IEEE Microwave Magazine, vol. 12, no. 7, pp. 78-94, 2011.

[2] M. A. Aldhaeebi, K. Alzoubi, T. S. Almoneef, S. M. Bamatraf, H. Attia, and O. M. Ramahi, "Review of microwaves techniques for breast cancer detection," Sensors, vol. 20, pp. 2390, 2020.

[3] R. C. Conceicao, J. Mohr, and M. O'Halloran, An Introduction to Microwave Imaging for Breast Cancer Detection, Biological and Medical Physics, Biomedical Engineering, Springer, 2016.

[4] N. Ghavami, G. Tiberi, D. J. Edwards, and A. Monorchio, "UWB microwave imaging of objects with canonical shape," IEEE Transactions on Antennas and Propagation, vol. 60, no. 1, pp. 231-239, 2012.

[5] A. Vispa, L. Sani, M. Paoli, A. Bigotti, G. Raspa, N. Ghavami, S. Caschera, M. Ghavami, M. Duranti, and G. Tiberi, "UWB device for breast microwave imaging: phantom and clinical validations," Measurement, vol. 146, pp. 582-589, 2019.

[6] L. Sani, N. Ghavami, A. Vispa, M. Paoli, G. Raspa, M. Ghavami, F. Sacchetti, E. Vannini, S. Ercolani, A. Saracini, M. Duranti, and G. Tiberi, "Novel microwave apparatus for breast lesions detection: Preliminary clinical results," Biomedical Signal Processing and control, vol. 52, pp. 257-263, 2019.

[7] American College of Radiology, ACR practice guideline for the performance of screening and diagnostic mammography, Practice Guidelines and Technical Standards, American College of Radiology, Reston, VA, USA, 2008.

[8] F. A. Tavassoli, P. Devilee, editors, World Health Classification of Tumours. Pathology and Genetics of Tumours of the Breast and Female Genital Organs, IARC press, Lyon, 2003.

[9] S. Lakhani, I. O. Ellis, S. J. Schnitt, et al. editors, WHO Classification of Tumour of the Breast, 4th edition, IARC, Lyon, 2012.

[10] N. Perry, M. Broeders, C. De Wolf, S. Trnberg, R. Holland, and L. von Karsa, European Guidelines for Quality Assurance in Breast Cancer Screening and Diagnosis, 4th edition, European Commission, 2006.

[11] D. Da Silva, M. Kaduri, M. Poley, O. Adir, N. Krinsky, J. Shainsky-Roitman, and A. Schroeder, "Biocompatibility, biodegradation and excretion of polylactic acid (PLA) in medical implants and theranostic systems," Chemical Engineering Journal, vol. 340, pp. 9-14, 2018.